ACADEMIC PRESS

Journal of Structural Biology 138 (2002) 21–33

Journal of Structural Biology

www.academicpress.com

# High-resolution electron microscopy and electron tomography: resolution versus precision

S. Van Aert,[a,*] A.J. den Dekker,[a] D. Van Dyck,[b] and A. van den Bos[a]

[a] *Department of Applied Physics, Delft University of Technology, Lorentzweg 1, 2628 CJ Delft, The Netherlands*
[b] *Department of Physics, University of Antwerp, Groenenborgerlaan 171, 2020 Antwerp, Belgium*

Received 28 November 2001; and in revised form 26 March 2002

**Abstract**

The performance of high-resolution electron microscopy and electron tomography is usually discussed in terms of two-point resolution, expressing the possibility of perceiving separately two image points of an object. However, the concept resolution obtains another meaning if one uses prior knowledge about the object and the imaging procedure in the form of a parametric model describing the expectations of the observations. The unknown parameters, such as the positions of the components in an object, can be measured quantitatively by fitting this model to the observations. Due to the statistical nature of the experiment, the resulting solutions for the positions of the components and therefore for the distance between the components will never be exact. An alternative to resolution is then the precision with which the distance can be measured. In the present paper, it is shown that the precision depends on the size of the components, the distance between the components, the resolution of the instrument, and the number of electron counts. For electron tomography, it also depends on the orientation of the object with respect to the rotation axis. 

*Keywords:* Electron tomography; High-resolution electron microscopy; Precision; Resolution

## 1. Introduction

The performance of high-resolution electron microscopy as well as of electron tomography is usually expressed in terms of two-point resolution. One of the earliest and most famous criteria for two-point resolution is that of Rayleigh. This criterion defines the possibility of perceiving separately two point sources in an image formed by a diffraction-limited imaging system or objective lens. According to Rayleigh, two point sources of equal brightness are just resolvable when the maximum of the intensity pattern produced by the first point source falls on the first zero of the intensity pattern produced by the second point source (Rayleigh, 1902). Consequently, the Rayleigh resolution limit is given by the distance between the central maximum and the first zero of the diffraction-limited intensity point-spread function of the imaging system concerned. Rayleigh's choice of resolution limit is based on presumed resolving capabilities of the human visual system when it is used to detect differences in intensity at various points of the composite intensity distribution. Since Rayleigh's days, several other resolution criteria have been proposed which are similar to Rayleigh's. Based on these so-called classical resolution criteria, it has been found, for example, that the resolution of an electron tomographic reconstruction is proportional to $1/J$, where $J$ is the total number of projections that is used for three-dimensional reconstruction (Crowther et al., 1970; Radermacher, 1992). Moreover, other parameters, such as the limited angular range, the magnification, and the defocus, limit the obtainable resolution (Grimm et al., 1998).

In fact, classical resolution criteria do not concern detected images but calculated images, that is, noise-free images exactly describable by a known parametric two-component mathematical model. The shape of the component function is assumed to be exactly known. However, classical resolution criteria disregard the possibility of using this a priori knowledge. Obviously,

* Corresponding author. Fax: +31-15-2784263.
*E-mail address:* s.vanaert@tn.tudelft.nl (S. Van Aert).

1047-8477/02/$ - see front matter 
PII: S1047-8477(02)00016-3

in the absence of noise, numerically fitting the known two-component model to the images with respect to the unknown parameters, for example, the positions of the two components, would result in a perfect fit. The resulting solution for the positions and therefore for the distance would be exact, and no limit to resolution would exist, no matter how closely spaced the two components. In reality, however, calculated images do not occur. Instead, one must deal with detected images. In this case, the model will never be known exactly and systematic errors are introduced. Furthermore, the images will never be noise-free, so that nonsystematic, or statistical, errors will also be present. These are the differences of each observation and its expectation. With respect to these nonsystematic errors, it is important, for example, for electron tomography, that the electron dose is high enough so as to obtain statistically significant image reconstructions (Hegerl and Hoppe, 1976). From this point of view, electron tomography tries to balance two conflicting requirements. On the one hand, in order to obtain a detailed and undistorted reconstruction, a tilt series must be recorded that covers as wide an angular range as possible in as many increments as possible. On the other hand, the electron dose must be kept subcritical if radiation damage is not to erase important details (Baumeister and Steven, 2000). However, ultimately, it is the systematic and nonsystematic errors that limit the resolution. An extensive survey on the concept resolution and on this consideration can be found in den Dekker and van den Bos (1997) and van den Bos and den Dekker (2001).

The present paper deals with nonsystematic errors only. Therefore, the parametric two-component model describing the expectations of the observations is assumed to be exactly known. The distance between the two components can be measured quantitatively by fitting this model to the images. However, if one would repeat this measurement several times, one would, due to the statistical nature of the experiment, find slightly different values for the distance, which are statistically distributed about the exact value. The variance of this distribution, or the standard deviation, which is defined as the square root of the variance, is then a measure for the precision of the distance. Use of the concept of Fisher information allows one to determine an expression for the highest attainable precision with which the distance can be measured, or equivalently, an expression for the lower bound on the attainable variance. The purpose of this paper is to approximate the exact expression with an analytical one, which is a useful rule of thumb for the attainable precision. This means that it is easy to calculate and to interpret so as to give more physical insight. The procedure is applied to one-, two-, and three-dimensional objects, for which the experiments consist of electron counting events in a one-dimensional, a two-dimensional, and a set of two-dimensional pixel arrays, respectively. The second experiment can be regarded as high-resolution electron microscopy and the third experiment as electron tomography.

The paper is organized as follows. In Section 2, the parametric model describing the expectations of the observations made at a one-, two-, and three-dimensional object is given. In Section 3, expressions for the highest attainable precision with which the distance can be measured and their approximations are derived. In Section 4, the approximations are compared with the exact expressions by means of a number of examples. In Section 5, conclusions are drawn.

## 2. Parametric model for the expectations of the observations

In this section, parametric models for the expectations of the observations made at one-, two-, and three-dimensional objects consisting of two identical components will be given. These models will be used in the derivation of expressions for the highest attainable precision with which the distance between the two components can be measured. The purpose is to find rules of thumb for the attainable precision, that is, expressions that are easy to calculate and to interpret. In order to accomplish this, it will be assumed that the models underlying the observations are the sum of two identical Gaussian functions. In practice, however, these models are of higher complexity. In that case, the rules of thumb will deviate from the exact expression. Nevertheless, they will still give physical insight.

The image intensity distribution of the one-dimensional object is described by

$$f(x;\beta) = \tfrac{1}{2}(F(x-\beta_{x1}) + F(x-\beta_{x2})), \tag{1}$$

where

$$F(x) = \frac{1}{\sqrt{2\pi}\rho}\exp\left(\frac{-x^2}{2\rho^2}\right). \tag{2}$$

The elements of the parameter vector $\beta = (\beta_1\,\beta_2)^{\mathrm{T}} = (\beta_{x1}\,\beta_{x2})^{\mathrm{T}}$ are the locations of the two components and $\rho$ is the width of the Gaussian peaks. The symbol T denotes taking the transpose. The width $\rho$ depends on the size of the components and on the resolution of the instrument. Suppose that the observations $w_k$, $k = 1,\ldots,K$ are made at equidistant pixels of length $\Delta x$ at the measurement points $x_k$. If $\Delta x$ is small enough, the probability $p_k(\beta)$ that an electron hits the pixel at the position $x_k$ is approximately given by

$$p_k(\beta) = p(x_k;\beta) = \int_{x_k-\Delta x/2}^{x_k+\Delta x/2} f(x;\beta)\,\mathrm{d}x \approx f(x_k;\beta)\Delta x. \tag{3}$$

This means that the number of electrons expected to be found at this pixel is given by $Np_k(\beta)$, where $N$ is the

total electron dose. Therefore, Eq. (3) defines the expectations of the observations $w_k$ recorded by the detector.

The image intensity distribution of the two-dimensional object is assumed to be given by

$$g(x,y;\beta) = \tfrac{1}{2}\big(G(x-\beta_{x1},y-\beta_{y1}) + G(x-\beta_{x2},y-\beta_{y2})\big), \tag{4}$$

where

$$G(x,y) = \frac{1}{2\pi\rho^2}\exp\left(\frac{-x^2-y^2}{2\rho^2}\right). \tag{5}$$

The elements of the parameter vector $\beta = (\beta_1\,\beta_2\,\beta_3\,\beta_4)^{\mathrm{T}} = (\beta_{x1}\,\beta_{x2}\,\beta_{y1}\,\beta_{y2})^{\mathrm{T}}$ are the locations of the two components and $\rho$ is the width of the Gaussian peaks. For a two-dimensional object, the components are, for example, atoms or atom columns in projection. In fact, Eq. (4) results from a two-dimensional convolution between an object function and the point spread function of the electron microscope. The intensity distribution of the two components of the object as well as the point spread function $t(x,y)$ is assumed to be Gaussian with corresponding widths $\rho_{\mathrm{C}}$ and $\rho_{\mathrm{EM}}$, respectively. In this case

$$\rho^2 = \rho_{\mathrm{C}}^2 + \rho_{\mathrm{EM}}^2. \tag{6}$$

The observations $w_{kl}$, $k = 1,\ldots,K$, $l = 1,\ldots,L$ are made at equidistant pixels of area $\Delta x \times \Delta y$ at the measurement points $(x_k, y_l)$. If $\Delta x$ and $\Delta y$ are small enough, the probability $p_{kl}(\beta)$ that an electron hits the pixel at the position $(x_k, y_l)$ is approximately given by

$$\begin{aligned} p_{kl}(\beta) &= p(x_k,y_l;\beta) \\ &= \int_{x_k-\Delta x/2}^{x_k+\Delta x/2}\int_{y_l-\Delta y/2}^{y_l+\Delta y/2} g(x,y;\beta)\,\mathrm{d}x\,\mathrm{d}y \\ &\approx g(x_k,y_l;\beta)\Delta x\Delta y. \end{aligned} \tag{7}$$

For a given total electron dose $N$, the number of electrons expected to be found at this pixel is given by $Np_{kl}(\beta)$. This result defines the expectations of the observations $w_{kl}$ recorded by the detector.

The observations made at the three-dimensional object consist of a single-axis tilt series of two-dimensional projections recorded by an electron tomography experiment. These projections are obtained by recording two-dimensional images while tilting the object around a fixed axis. Other data collection geometries in electron tomography exist as well, such as conical and random-conical tilting. However, only single-axis tilting will be considered in the present paper. It will be assumed that the three-dimensional density distribution of the object is given by

$$\begin{aligned} \mathrm{d}(x,y,z;\beta) = \tfrac{1}{2}\big(&D(x-\beta_{x1},y-\beta_{y1},z-\beta_{z1}) \\ &+ D(x-\beta_{x2},y-\beta_{y2},z-\beta_{z2})\big), \end{aligned} \tag{8}$$

where

$$D(x,y,z) = \frac{1}{(2\pi)^{3/2}\rho_{\mathrm{C}}^3}\exp\left(\frac{-x^2-y^2-z^2}{2\rho_{\mathrm{C}}^2}\right). \tag{9}$$

The elements of the parameter vector $\beta = (\beta_1\,\beta_2\,\beta_3\,\beta_4\,\beta_5\,\beta_6)^{\mathrm{T}} = (\beta_{x1}\,\beta_{x2}\,\beta_{y1}\,\beta_{y2}\,\beta_{z1}\,\beta_{z2})^{\mathrm{T}}$ are the locations of the two components with respect to a reference coordinate system and $\rho_{\mathrm{C}}$ is the width of the components. The components are, for example, atoms. Fig. 1 shows the surface of the three-dimensional density distribution and the locations of the two components. It will be assumed that the $y$-axis is the rotation axis and the $z$-axis is the axis parallel to the illuminating electron beam. In the derivation of a rule of thumb for the attainable precision, it will be assumed that the tilt angles $\theta^j$, $j = 1,\ldots,J$ are equidistantly sampled at the interval $(-\pi/2, \pi/2)$. Although a full angular range is rather unrealistic, it will be shown in Section 4 that the derived rule of thumb still provides physical insight in case of a limited angular range. At each tilt angle $\theta^j$, the locations of the two components $\beta^j = (\beta_{x1}^j\,\beta_{x2}^j\,\beta_{y1}^j\,\beta_{y2}^j\,\beta_{z1}^j\,\beta_{z2}^j)^{\mathrm{T}}$ with respect to the reference coordinate system are given by

$$\begin{aligned} \beta_{x1}^j &= \beta_{x1}\cos\theta^j + \beta_{z1}\sin\theta^j, \\ \beta_{x2}^j &= \beta_{x2}\cos\theta^j + \beta_{z2}\sin\theta^j, \\ \beta_{y1}^j &= \beta_{y1}, \\ \beta_{y2}^j &= \beta_{y2}, \\ \beta_{z1}^j &= \beta_{z1}\cos\theta^j - \beta_{x1}\sin\theta^j, \\ \beta_{z2}^j &= \beta_{z2}\cos\theta^j - \beta_{x2}\sin\theta^j. \end{aligned} \tag{10}$$

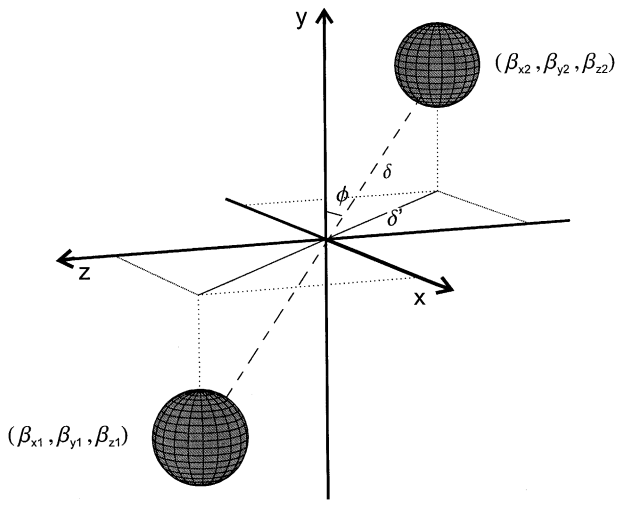


Fig. 1. Surface of the three-dimensional density distribution of an object consisting of two components. The locations of the two components are represented by the elements of the parameter vector $\beta$. It has been assumed that the $y$-axis is the rotation axis and the $z$-axis is the axis parallel to the illuminating electron beam. Furthermore, $\delta$ is the distance between the two components, $\delta'$ is the distance between the components projected onto the $(x,z)$-plane, and $\phi$ is the angle between the rotation axis and the axis connecting both components. Notice that this is not the tilt angle.

The image intensity distribution of a two-dimensional projection is equal to

$$h^j(x,y;\beta) = \int \mathrm{d}(x,y,z;\beta^j)\,\mathrm{d}z * t(x,y) = g(x,y;\epsilon^j), \quad (11)$$

that is, the convolution of the projected density distribution and the point spread function of the electron microscope. The parameters $\epsilon^j = (\beta^j_{x1}\,\beta^j_{x2}\,\beta^j_{y1}\,\beta^j_{y2})^{\mathrm{T}}$ are the locations of the components in this projection and the function $g$ is given by Eq. (4). The observations $w^j_{kl}$, $k = 1,\ldots,K$, $l = 1,\ldots,L$, $j = 1,\ldots,J$ are made at equidistant pixels of area $\Delta x \times \Delta y$ at the measurement points $(x_k, y_l)$ at the tilt angle $\theta^j$. If $\Delta x$ and $\Delta y$ are small enough, the probability $p^j_{kl}(\beta)$ that an electron hits the pixel at the position $(x_k, y_l)$ at the tilt angle $\theta^j$ is approximately given by

$$\begin{aligned} p^j_{kl}(\beta) &= p^j(x_k, y_l; \beta) \\ &= \int_{x_k-\Delta x/2}^{x_k+\Delta x/2} \int_{y_l-\Delta y/2}^{y_l+\Delta y/2} h^j(x,y;\beta)\,\mathrm{d}x\,\mathrm{d}y \\ &\approx h^j(x_k, y_l; \beta)\Delta x \Delta y. \end{aligned} \quad (12)$$

It will be assumed that the total electron dose $N$ is equally distributed over the two-dimensional projections. In this case, the electron dose at each projection is equal to $N/J$. The number of electrons expected to be found at the pixel at the position $(x_k, y_l)$ at the tilt angle $\theta^j$ is then given by $(N/J)p^j_{kl}(\beta)$. This result defines the expectations of the observations $w^j_{kl}$ recorded by the detector.

The parametric two-component models describing the expectations of the observations, which are given in this section, will be used in the derivation of the statistical precision with which the distance between the two components can be measured.

## 3. Statistical measurement precision

In the preceding section, two-component models describing the expectations of the observations made at one-, two-, and three-dimensional objects were derived. These models are parametric in the locations of the components. In what follows, it will be shown how these location parameters enter the probability density function of the statistical observations. From this parameterized probability density function, the Cramér–Rao Lower Bound may be computed (van den Bos, 1982; van den Bos and den Dekker, 2001). This is a lower bound on the variance of the location parameters. For the purpose of this paper, the most important parameter is the distance between the components. Therefore, an expression for the Cramér–Rao Lower Bound on the variance of the distance will be derived. It follows relatively easily from the Cramér–Rao Lower Bound on the variance of the location parameters.

### 3.1. The joint probability density function of the observations

Any electron microscopist will readily admit that his or her observations "contain errors." These errors must be specified. This specification is the subject of this subsection.

Generally, sets of observations made under the same conditions nevertheless differ from experiment to experiment. The usual way to describe this behavior is to model the observations as stochastic variables. The reason is that there is no viable alternative and that it has been found to work. Stochastic variables are defined by probability density functions (van den Bos and den Dekker, 2001). In an electron microscopy experiment the observations are electron counting results, for which the probability density function can be modeled as a Poisson distribution.

Consider a set of stochastic observations $w_m$, $m = 1,\ldots,M$. Then the vector $w$ defined as

$$w = (w_1 \ldots w_M)^{\mathrm{T}} \quad (13)$$

represents the $M \times 1$ column vector of these observations. From the assumptions made in Section 2, it follows that the number of observations $M$ made at the one-, two-, and three-dimensional object is equal to $K$, $K \times L$, and $K \times L \times J$, respectively. The observations are assumed to be statistically independent and have a Poisson distribution. Therefore, the probability that the observation $w_m$ is equal to $\omega_m$ is given by (Mood et al., 1974)

$$\frac{\lambda_m^{\omega_m}}{\omega_m!}\exp(-\lambda_m), \quad (14)$$

where the parameter $\lambda_m$ is equal to the expectation $E[w_m]$. The expectation values $E[w_m]$ are equal to

$$E[w_m] = \lambda_m = np_m(\beta), \quad (15)$$

where the number of electrons $n$ is equal to $N$, $N$, and $N/J$ and the probability $p_m$ that an electron hits a pixel is given by Eqs. (3), (7), and (12) for the parametric models of the one-, two-, and three-dimensional object, respectively. Since the $w_m$ are assumed to be independent, the probability $P(\omega;\beta)$ of a set of observations $\omega = (\omega_1 \ldots \omega_M)^{\mathrm{T}}$ is the product of all probabilities described by Eq. (14):

$$P(\omega;\beta) = \prod_{m=1}^{M} \frac{\lambda_m^{\omega_m}}{\omega_m!}\exp(-\lambda_m). \quad (16)$$

This function is called the joint probability density function of the observations. From Eq. (15), it follows that the location parameters $\beta$ enter $P(\omega;\beta)$ via $\lambda_m$. In the following subsection, the joint probability density function will be used for the computation of the Cramér–Rao Lower Bound.

### 3.2. The Cramér–Rao Lower Bound

In this subsection, the Cramér–Rao Lower Bound is discussed. This is a lower bound on the variance of any unbiased estimator. What does this mean? Suppose that an experimenter wants to measure the location parameters $\beta$ of two components or the distance $\delta$ between two components quantitatively. For this purpose, one can use many estimators (estimation methods), such as least squares, least absolute values, or maximum likelihood estimators. The precision of an estimator is represented by the variance or by the standard deviation. Generally, different estimators will have different precisions. It can be shown, however, that the variance of unbiased estimators will never be lower than the Cramér–Rao Lower Bound. Fortunately, there exists a class of estimators (including the maximum likelihood estimator) that achieves this bound at least asymptotically, that is, for the number of observations going to infinity. The details of this lower bound can be found in van den Bos and den Dekker (2001) and van den Bos (1982).

First, the Fisher information matrix $F$ with respect to the elements of the parameter vector $\beta$ is introduced. If $D$ represents the dimension of the object, the Fisher information matrix is defined as the $2D \times 2D$ matrix

$$F = -E\left[\frac{\partial^2 \ln P(\omega;\beta)}{\partial\beta\partial\beta^{\mathrm{T}}}\right]. \tag{17}$$

In this expression $P(\omega;\beta)$ is defined by Eq. (16) and $\partial^2 \ln P(\omega;\beta)/\partial\beta\partial\beta^{\mathrm{T}}$ represents the Hessian matrix of ln $P$ defined by its $(r,s)$th element $\partial^2 \ln P(\omega;\beta)/\partial\beta_r\partial\beta_s$. From Eqs. (15)–(17) it follows that the elements $F_{rs}$ are equal to

$$F_{rs} = n\sum_{m=1}^{M}\frac{1}{p_m}\frac{\partial p_m}{\partial\beta_r}\frac{\partial p_m}{\partial\beta_s}. \tag{18}$$

Next, it can be shown that the covariance matrix cov $(b)$ of any unbiased estimator $b$ of $\beta$ satisfies

$$\mathrm{cov}(b) \geqslant F^{-1}. \tag{19}$$

This inequality expresses that the difference of cov $(b)$ and $F^{-1}$ is positive semidefinite. Since the diagonal elements of cov $(b)$ represent the variances of $b_1,\ldots,b_{2D}$ and since the diagonal elements of a positive semidefinite matrix are nonnegative, these variances are larger than or equal to the corresponding diagonal elements of $F^{-1}$. In this sense, $F^{-1}$ represents a lower bound to the variances of all unbiased $b$. The matrix $F^{-1}$ is called the Cramér–Rao Lower Bound on the variance of $b$.

Finally, the Cramér–Rao Lower Bound can be extended to include unbiased estimators of vectors of functions of the parameters instead of the parameters proper. Let $\gamma(\beta) = (\gamma_1(\beta)\ldots\gamma_L(\beta))$ be such a vector and let $c = (c_1\ldots c_L)^{\mathrm{T}}$ be an unbiased estimator of $\gamma(\beta)$. Then it can be shown that

$$\mathrm{cov}(c) \geqslant \frac{\partial\gamma}{\partial\beta^{\mathrm{T}}}F^{-1}\frac{\partial\gamma^{\mathrm{T}}}{\partial\beta}, \tag{20}$$

where $\partial\gamma/\partial\beta^{\mathrm{T}}$ is the $L \times 2D$ Jacobian matrix defined by its $(r,s)$th element $\partial\gamma_r/\partial\beta_s$ (van den Bos, 1982). The right-hand side member of this inequality is the Cramér–Rao Lower Bound on the variance of $c$ and its inverse is the Fisher information matrix with respect to the elements of the parameter vector $\gamma$. Expression (20) will be used in the derivation of the Cramér–Rao Lower Bound on the variance of the distance between two components.

### 3.3. Approximations of the Cramér–Rao Lower Bound

In this subsection, rules of thumb will be derived for the highest attainable precision with which the distance between two components can be measured. In other words, the exact expressions for the Cramér–Rao Lower Bound, following from Section 3.2, will be approximated. This will be done for one-, two-, and three-dimensional objects, for which the observations are electron counting events. The parametric models describing the expectations of these observations are given in Section 2.

#### 3.3.1. One-dimensional object

For a one-dimensional object, an approximation of the Cramér–Rao Lower Bound $\sigma_\delta^2$ on the variance of the distance $\delta$ between the two components was derived in Bettens et al. (1999)

$$\sigma_\delta^2 \approx \frac{8\rho^4}{N\delta^2} \quad \text{if } \delta \leqslant \sqrt{2}\rho, \tag{21}$$

$$\sigma_\delta^2 \approx \frac{4\rho^2}{N} \quad \text{if } \delta \geqslant \sqrt{2}\rho. \tag{22}$$

If $\delta$ is equal to $\sqrt{2}\rho$, both approximations are equal to each other. In the derivation of Eqs. (21) and (22), it has been assumed that the observations are multinomially distributed instead of Poisson distributed. However, the expressions for the elements of the Fisher information matrix, which are given in Eq. (18), are equal under both assumptions. Therefore, also the approximations of $\sigma_\delta^2$ are equal. From Eqs. (21) and (22), it follows that the precision with which the distance can be measured is a function of the total number of electrons, the distance between the components, and the width of the peaks. The precision can be increased, that is, $\sigma_\delta^2$ can be decreased, by increasing the number of electrons. Also, the precision will be higher if the width of the peaks is smaller or if the components are further separated. In Bettens et al. (1999), it has been shown that the approximations given in Eqs. (21) and (22) are useful rules of thumb.

*3.3.2. Two-dimensional object*

For a two-dimensional object, a rule of thumb for the highest attainable precision with which the distance between two components can be measured will be derived by making a number of approximations. The derivation is similar to that of the one-dimensional object.

First, it has been assumed that the two-dimensional object is located for the most part within the region of observation. In this case, $F_{11} \approx F_{22}$, $F_{33} \approx F_{44}$, $F_{24} \approx F_{13}$, and $F_{23} \approx F_{14}$. Furthermore, it follows from Eq. (18) that $F$ is symmetric. Therefore, $F$ simplifies into

$$F \approx \begin{pmatrix} F_{11} & F_{12} & F_{13} & F_{14} \\ F_{12} & F_{11} & F_{14} & F_{13} \\ F_{13} & F_{14} & F_{33} & F_{34} \\ F_{14} & F_{13} & F_{34} & F_{33} \end{pmatrix}. \tag{23}$$

The purpose of this paper is to find an expression for the Cramér–Rao Lower Bound on the variance of the distance between two components. For a two-dimensional object, the distance is defined as

$$\delta = \sqrt{(\beta_{x1} - \beta_{x2})^2 + (\beta_{y1} - \beta_{y2})^2}. \tag{24}$$

Since $\delta$ is a function of the elements of the parameter vector $\beta$, an expression for the Cramér–Rao Lower Bound follows directly from the right-hand side member of inequality (20). However, in order to simplify the calculations, an additional transformation of the location parameters into a new set of parameters $\alpha$ has been performed. The elements of the parameter vector $\alpha = (\alpha_1\ \alpha_2\ \alpha_3\ \alpha_4)^{\mathrm{T}}$ are defined as

$$\begin{aligned} \alpha_1 &= \beta_{x1} - \beta_{x2}, \\ \alpha_2 &= \beta_{y1} - \beta_{y2}, \\ \alpha_3 &= \beta_{x1} + \beta_{x2}, \\ \alpha_4 &= \beta_{y1} + \beta_{y2}. \end{aligned} \tag{25}$$

The Fisher information matrix $F_\alpha$ with respect to the elements of the parameter vector $\alpha$ follows from taking the inverse of the right-hand side member of inequality (20)

$$F_\alpha = \left( \frac{\partial \alpha}{\partial \beta^{\mathrm{T}}} F^{-1} \frac{\partial \alpha^{\mathrm{T}}}{\partial \beta} \right)^{-1} = \left( \frac{\partial \alpha^{\mathrm{T}}}{\partial \beta} \right)^{-1} F \left( \frac{\partial \alpha}{\partial \beta^{\mathrm{T}}} \right)^{-1}. \tag{26}$$

From Eqs. (23), (25), and (26) it follows that $F_\alpha$ is a block diagonal matrix, represented by

$$F_\alpha \approx \frac{1}{2} \begin{pmatrix} F_{11} - F_{12} & F_{13} - F_{14} & 0 & 0 \\ F_{13} - F_{14} & F_{33} - F_{34} & 0 & 0 \\ 0 & 0 & F_{11} + F_{12} & F_{13} + F_{14} \\ 0 & 0 & F_{13} + F_{14} & F_{33} + F_{34} \end{pmatrix}. \tag{27}$$

Next, the Cramér–Rao Lower Bound $\sigma_\delta^2$ on the variance of $\delta$ can be calculated from the right-hand side member of inequality (20)

$$\sigma_\delta^2 = \frac{\partial \delta}{\partial \alpha^{\mathrm{T}}} F_\alpha^{-1} \frac{\partial \delta^{\mathrm{T}}}{\partial \alpha}. \tag{28}$$

From Eqs. (24) and (25), it follows that $\delta$ can be written as a function of the elements of the parameter vector $\alpha$

$$\delta = \sqrt{\alpha_1^2 + \alpha_2^2}. \tag{29}$$

From this equation it follows that the Jacobian matrix $\partial\delta/\partial\alpha^{\mathrm{T}}$ is equal to

$$\frac{\partial \delta}{\partial \alpha^{\mathrm{T}}} = \frac{1}{\delta}(\alpha_1\ \alpha_2\ 0\ 0). \tag{30}$$

From Eqs. (27), (28), and (30) and since $F_\alpha$ is block diagonal, it follows that

$$\sigma_\delta^2 \approx \frac{2}{\delta^2}(\alpha_1 \alpha_2) \begin{pmatrix} F_{11} - F_{12} & F_{13} - F_{14} \\ F_{13} - F_{14} & F_{33} - F_{34} \end{pmatrix}^{-1} \begin{pmatrix} \alpha_1 \\ \alpha_2 \end{pmatrix}. \tag{31}$$

Finally, Eq. (31) has been calculated explicitly in Appendix A for the special cases where the distance between the two components is small or large. This results in the following rules of thumb

$$\sigma_\delta^2 \approx \frac{8\rho^4}{N\delta^2} \quad \text{if } \delta \leqslant \sqrt{2}\rho, \tag{32}$$

$$\sigma_\delta^2 \approx \frac{4\rho^2}{N} \quad \text{if } \delta \geqslant \sqrt{2}\rho. \tag{33}$$

If $\delta$ is equal to $\sqrt{2}\rho$, both approximations are equal to each other. Eqs. (32) and (33) are also equal to their one-dimensional analogues, which are given in Eqs. (21) and (22). From these approximations, it follows that the precision with which the distance can be measured is a function of both the total number of electrons and the width of the peaks. The attainable precision will be higher if the width of the peaks is smaller. In practice, it follows from Eq. (6) that this can be realized by improving the resolution of the electron microscope. However, it is important to notice that beyond a certain point, it will be useless to further improve the resolution, since then, the width of the peaks is determined by the width of the components, for example, by the width of the electrostatic potential of the atoms (den Dekker et al., 1999). If the total number of electrons is large, the precision can be orders of magnitude better than the resolution. If the distance becomes smaller than $\sqrt{2}\rho$, the standard deviation $\sigma_\delta$ increases inversely proportionally to the distance. In a sense $\sigma_\delta$ is the "error bar" on the distance. In Section 4, it will be shown that $\sigma_\delta$ is well approximated by the square roots of the right-hand side members of Eqs. (32) and (33).

*3.3.3. Three-dimensional object*

The derivation of a rule of thumb for the highest attainable precision with which the distance between

two components of a three-dimensional object can be measured is similar to its two-dimensional analogue. It should be made clear that the interpretation of this measurement is as follows. The distance is measured by fitting the assembly of projected models, given in Eq. (12), to the projected images, using a criterion of goodness of fit. This procedure is preferred to fitting the three-dimensional model, such as that given in Eq. (8), to a three-dimensional reconstruction. The reason for this preference is that the joint probability density function of the reconstruction is not known. Nevertheless, the reconstruction is needed in order to provide good starting values for the parameters in quantitative structure determination. This can be illustrated as follows. Quantitative structure determination is done in an iterative optimization procedure. At each iteration, the parameters are slightly changed in order to improve the goodness of fit. With respect to this refinement procedure, it is important to have good starting values for the parameters so as to avoid ending up at a local optimum, instead of at the global optimum of the criterion of goodness of fit.

The three-dimensional object is assumed to be located for the most part within the region of observation. Furthermore, the Fisher information matrix is a symmetric matrix. Therefore, it can be shown that

$$F \approx \begin{pmatrix} F_{11} & F_{12} & F_{13} & F_{14} & F_{15} & F_{16} \\ F_{12} & F_{11} & F_{14} & F_{13} & F_{16} & F_{15} \\ F_{13} & F_{14} & F_{33} & F_{34} & F_{35} & F_{36} \\ F_{14} & F_{13} & F_{34} & F_{33} & F_{36} & F_{35} \\ F_{15} & F_{16} & F_{35} & F_{36} & F_{55} & F_{56} \\ F_{16} & F_{15} & F_{36} & F_{35} & F_{56} & F_{55} \end{pmatrix}. \tag{34}$$

Subsequently, the location parameters are transferred into a new set of parameters $\alpha = (\alpha_1\alpha_2\alpha_3\alpha_4\alpha_5\alpha_6)^{\mathrm{T}}$ defined as

$$\begin{aligned} \alpha_1 &= \beta_{x1} - \beta_{x2}, \\ \alpha_2 &= \beta_{y1} - \beta_{y2}, \\ \alpha_3 &= \beta_{z1} - \beta_{z2}, \\ \alpha_4 &= \beta_{x1} + \beta_{x2}, \\ \alpha_5 &= \beta_{y1} + \beta_{y2}, \\ \alpha_6 &= \beta_{z1} + \beta_{z2}. \end{aligned} \tag{35}$$

Following the same lines of thought as in the derivation of Eq. (27), it can be shown that the Fisher information matrix $F_\alpha$ is block diagonal and given by

$$F_\alpha \approx \frac{1}{2}\begin{pmatrix} F_{11}-F_{12} & F_{13}-F_{14} & F_{15}-F_{16} & 0 & 0 & 0 \\ F_{13}-F_{14} & F_{33}-F_{34} & F_{35}-F_{36} & 0 & 0 & 0 \\ F_{15}-F_{16} & F_{35}-F_{36} & F_{55}-F_{56} & 0 & 0 & 0 \\ 0 & 0 & 0 & F_{11}+F_{12} & F_{13}+F_{14} & F_{15}+F_{16} \\ 0 & 0 & 0 & F_{13}+F_{14} & F_{33}+F_{34} & F_{35}+F_{36} \\ 0 & 0 & 0 & F_{15}+F_{16} & F_{35}+F_{36} & F_{55}+F_{56} \end{pmatrix}. \tag{36}$$

The distance parameter $\delta$, written as a function of the elements of the parameter $\alpha$, is equal to

$$\delta = \sqrt{\alpha_1^2 + \alpha_2^2 + \alpha_3^2}. \tag{37}$$

From the right-hand side member of inequality (20), it can be derived that the Cramér–Rao Lower Bound $\sigma_\delta^2$ on the variance of $\delta$ is given by

$$\sigma_\delta^2 \approx \frac{2}{\delta^2}\begin{pmatrix} \alpha_1 & \alpha_2 & \alpha_3 \end{pmatrix} \times \begin{pmatrix} F_{11}-F_{12} & F_{13}-F_{14} & F_{15}-F_{16} \\ F_{13}-F_{14} & F_{33}-F_{34} & F_{35}-F_{36} \\ F_{15}-F_{16} & F_{35}-F_{36} & F_{55}-F_{56} \end{pmatrix}^{-1} \begin{pmatrix} \alpha_1 \\ \alpha_2 \\ \alpha_3 \end{pmatrix}. \tag{38}$$

Eq. (38) has been calculated explicitly in Appendix B for the special cases where the distance between the two components is small or large. This results in the following rules of thumb

$$\sigma_\delta^2 \approx \frac{8\rho^4}{N\delta^2} V(\phi) \quad \text{if } \delta \leqslant \sqrt{2V(\phi)/W(\phi)}\rho, \tag{39}$$

$$\sigma_\delta^2 \approx \frac{4\rho^2}{N} W(\phi) \quad \text{if } \delta \geqslant \sqrt{2V(\phi)/W(\phi)}\rho, \tag{40}$$

where

$$V(\phi) = 4\frac{3\cos^4\phi - 3\cos^2\phi - 2}{\cos^4\phi - 6\cos^2\phi - 3}, \tag{41}$$

$$W(\phi) = 1 + \sin^2\phi, \tag{42}$$

and $\phi$ is the angle between the rotation axis and the axis that connects the two components. This angle has been visualized in Fig. 1. Notice that this is not the tilt angle. For different tilt angles $\theta'$ in a tilt series, $\phi$ is constant. If $\delta$ is equal to $\sqrt{2V(\phi)/W(\phi)}\rho$, for a given angle $\phi$, both approximations are equal to each other. From Eqs. (39) and (40), it follows that the precision with which the distance can be measured is a function of the total number of electrons, the width of the peaks, the distance between the components, and the angle $\phi$. If $\phi$ is equal to $\pi/2$, the approximated $\sigma_\delta^2$ is about two times as large as if $\phi$ is equal to 0. In terms of the standard deviation this corresponds to a factor $\sqrt{2}$. If $\phi$ is equal to 0, the approximations given in Eqs. (39) and (40) are equal to their two-dimensional analogues given in Eqs. (32) and (33). This is intuitively clear since in this case the

components are on the rotation axis and therefore the distance between the components in a two-dimensional projection is at each tilt angle equal to the real distance. In Section 4, it will be shown that the square roots of the right-hand side members of Eqs. (39) and (40) describe the exact values $\sigma_\delta$ sufficiently accurately.

## 4. Discussions and examples

In this section, the exactly calculated standard deviation $\sigma_\delta$ will be compared with its approximations for two- and three-dimensional objects. For the one-dimensional object, a discussion can be found in Bettens et al. (1999).

First, the approximations of the standard deviation of the distance, given by the square roots of the right-hand side members of Eqs. (32) and (33), will be investigated by means of examples. Fig. 2 shows the exactly calculated $\sigma_\delta$ and its approximations as a function of the distance between the two components. It can be observed that the square roots of the right-hand side members of Eqs. (32) and (33) are accurate approximations of $\sigma_\delta$ for distances smaller than and larger than $\sqrt{2}\rho$, respectively. This figure is an example to illustrate that these approximations are useful rules of thumb. One of the assumptions that has been made in the derivation is that the pixel sizes $\Delta x$ and $\Delta y$ are small. Therefore, Fig. 3 shows the exactly calculated $\sigma_\delta$ as a function of the pixel size $\Delta x$, which has been assumed to be equal to $\Delta y$. From Fig. 3, it can be seen that below a certain pixel size, $\sigma_\delta$ decreases only slightly with decreasing pixel size, with all other quantities kept constant. This means that the precision that can be gained by decreasing the pixel size is only marginal.

Second, the approximations of the standard deviation of the distance, given by the square roots of the right-hand side members of Eqs. (39) and (40), are discussed. Fig. 4 shows the exactly calculated $\sigma_\delta$ from 20 projected images and its approximations as a function of the distance between the two components. The axis combining both components is supposed to be perpendicular to the rotation axis. The square roots of the right-hand side members of Eqs. (39) and (40) are accurate approximations of $\sigma_\delta$ for distances smaller than and larger than $\sqrt{2V(\pi/2)/W(\pi/2)}\rho$, respectively. In Figs. 5 and 6, the exactly calculated $\sigma_\delta$ from 20 projected images and its approximations are shown as a function of the angle $\phi$ for the cases where the distance between the components is small and large, respectively. The behavior of $\sigma_\delta$ is accurately described by the square roots of the functions $V(\phi)$ and $W(\phi)$, which are given in Eqs. (41) and (42), respectively. The examples given in Figs. 4–6 illustrate that Eqs. (39) and (40) are useful rules of thumb.

Finally, some remarks are due. It should be noticed that in the derivation of the approximations, which is

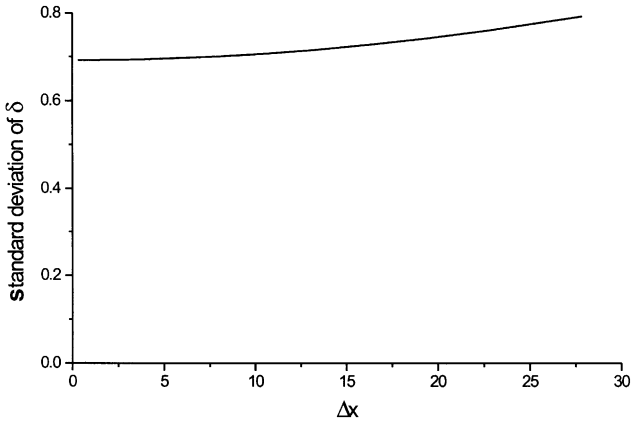


Fig. 3. The exactly calculated $\sigma_\delta$ of a two-dimensional object as a function of the pixel size $\Delta x$, with $\Delta y = \Delta x$, $N = 30000$, $\rho = 20$, and $\delta = 10$.

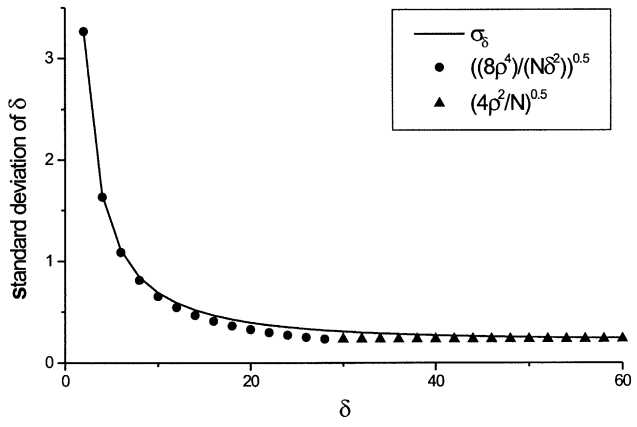


Fig. 2. The exactly calculated $\sigma_\delta$ of a two-dimensional object and its approximations, given by the square roots of the right-hand side members of Eqs. (32) and (33), as a function of the distance between the two components, with $N = 30000$, $\rho = 20$, and $\Delta x = \Delta y = 1.2$.

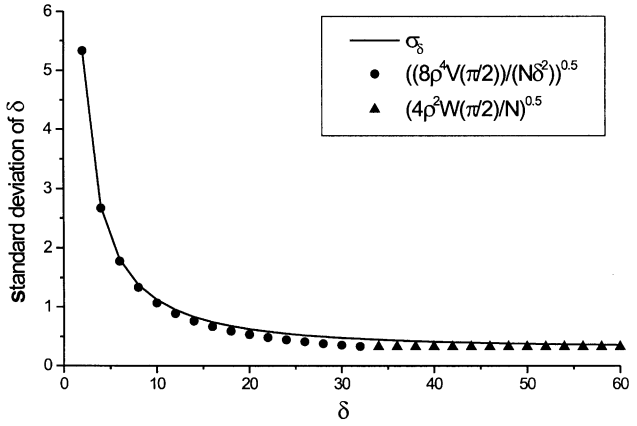


Fig. 4. The exactly calculated $\sigma_\delta$ from 20 projected images of a three-dimensional object and its approximations, given by the square roots of the right-hand side members of Eqs. (39) and (40), as a function of the distance between the two components, with $N = 30000$, $\rho = 20$, $\phi = \pi/2$, and $\Delta x = \Delta y = 1.2$.

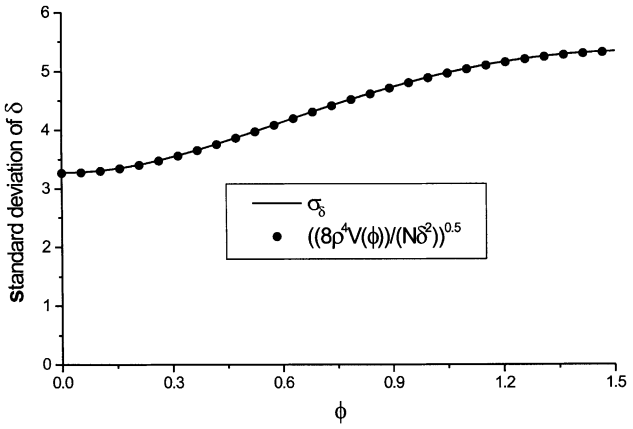


Fig. 5. The exactly calculated $\sigma_\delta$ from 20 projected images of a three-dimensional object and its approximation, given by the square root of the right-hand side member of Eq. (39), as a function of the angle between the rotation axis and the axis connecting the two components of the object, with $N = 30000$, $\rho = 20$, $\delta = 2$, and $\Delta x = \Delta y = 1.2$.

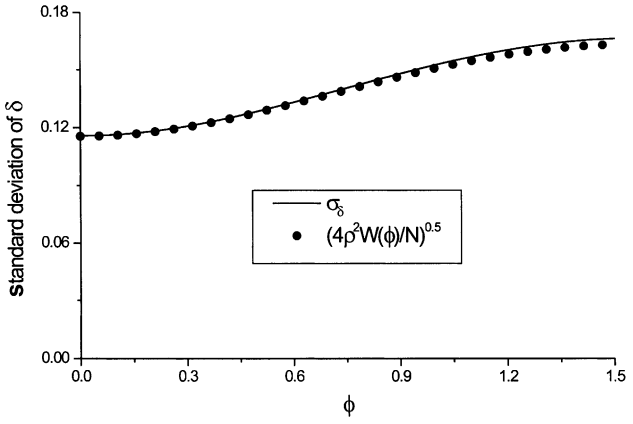


Fig. 6. The exactly calculated $\sigma_\delta$ from 20 projected images of a three-dimensional object and its approximation, given by the square root of the right-hand side member of Eq. (40), as a function of the angle between the rotation axis and the axis connecting the two components of the object, with $N = 30000$, $\rho = 10$, $\delta = 50$, and $\Delta x = \Delta y = 1.2$.

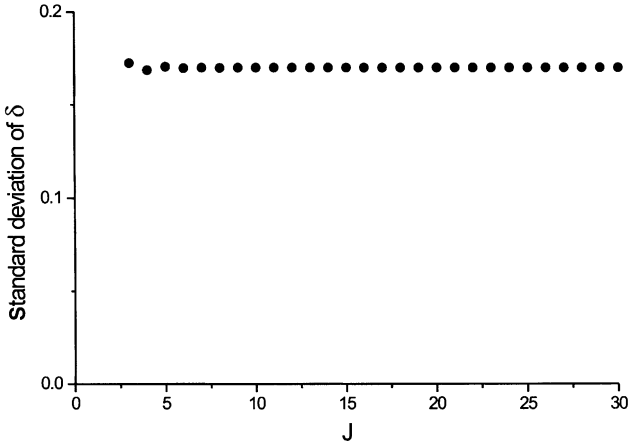


Fig. 7. The exactly calculated $\sigma_\delta$ of a three-dimensional object as a function of the number of projections, with $N = 30000$, $\rho = 10$, $\phi = \pi/2$, $\delta = 40$, and $\Delta x = \Delta y = 1.2$.

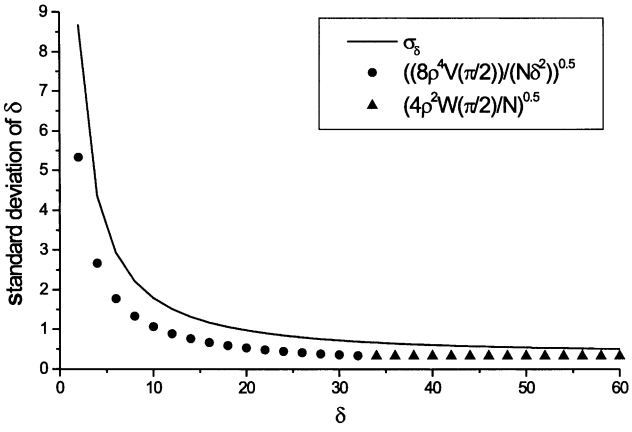


Fig. 8. The exactly calculated $\sigma_\delta$ from 20 projected images of a three-dimensional object assuming a limited angular tilt range, that is, the interval $(-\pi/3, \pi/3)$, and its approximations, given by the square roots of the right-hand side members of Eqs. (39) and (40), as a function of the distance between the two components, with $N = 30000$, $\rho = 20$, $\phi = \pi/2$, and $\Delta x = \Delta y = 1.2$.

given in the appendices, the total number of projections has been assumed to be large, which is rather unrealistic. However, in the comparisons presented in Figs. 4–6, the exactly calculated $\sigma_\delta$ follows from the assumption that there are only 20 available projections. This shows that the approximations are useful, even for a limited number of projections. Moreover, Fig. 7 shows the exactly calculated $\sigma_\delta$ as a function of the total number of projections, with all other parameters kept constant. It can be seen that there is a fast convergence of $\sigma_\delta$ to a constant with increasing number of projections. This means that the precision does not improve beyond a certain number of projections. Furthermore, in the derivation of the approximations, a full angular tilt range has been assumed, which is also unrealistic. Therefore, Fig. 8 shows the exactly calculated $\sigma_\delta$, following from a limited angular tilt range, that is, the interval $(-\pi/3, \pi/3)$, and the approximations as a function of the distance between the two components. Although the approximations start to deviate from the exactly calculated $\sigma_\delta$, they are still useful as a general rule of thumb since they describe the behavior of $\sigma_\delta$ well.

## 5. Conclusion

In this work, the performance of high-resolution electron microscopy and electron tomography has been discussed in terms of the statistical precision with which the distance between two components can be measured. Unlike classical two-point resolution criteria, this alternative performance measure takes object and dose

aspects into account. The purpose was to find rules of thumb for the precision, that is, expressions that are easy to calculate and to interpret so as to give more physical insight. In order to accomplish this, simplified models for the expectations of the observations have been proposed. From these rules of thumb, it follows that the precision is a function of the resolution of the electron microscope, the size of the components, the total number of detected electrons, and the distance between the two components. The precision can be improved by increasing the total number of detected electrons or by improving the resolution of the electron microscope. However, beyond a certain point, the precision is limited by the intrinsic size of the components. Then it is useless to further improve the resolution of the electron microscope. For electron tomography, the precision also depends on the orientation of the object with respect to the rotation axis. Furthermore, the precision does not improve by increasing the number of projections beyond a certain number. Finally, it should be noticed that the discussion about resolution versus precision is not specific to electron microscopy; it is important in a wide variety of applications.

## Acknowledgments

The research of Dr. A.J. den Dekker has been made possible by a fellowship of the Royal Netherlands Academy of Arts and Sciences (KNAW).

## Appendix A

In this appendix, the approximations, given in Eqs. (32) and (33), for the highest attainable precision with which the distance between two components of a two-dimensional object can be estimated will be derived. First, Eq. (32), which is valid if $\delta$ is small compared to $\rho$, will be proven. The proof is similar to its one-dimensional analogue, which has been derived in Bettens et al. (1999). From Eq. (18), it follows that:

$$F_{11}-F_{12}\approx\frac{N}{2}\sum_{k=1}^{K}\sum_{l=1}^{L}\frac{1}{p_{kl}}\left(\frac{\partial p_{kl}}{\partial\beta_{x1}}-\frac{\partial p_{kl}}{\partial\beta_{x2}}\right)^2, \tag{A.1}$$

where it has been taken into account that $F_{11}\approx F_{22}$ and $F_{12}=F_{21}$. The number of electrons $n$ and the summation over $m$ in Eq. (18) have been replaced by the total number of electrons $N$ and the summations over $k$ and $l$. The derivatives $\partial p_{kl}/\partial\beta_{x1}$ and $\partial p_{kl}/\partial\beta_{x2}$ can be rewritten, using Eqs. (4), (7), and (25), as

$$\frac{\partial p_{kl}}{\partial\beta_{x1}}\approx-\frac{1}{2}\frac{\partial G(x_k-(\alpha_1+\alpha_3)/2,y_l-(\alpha_2+\alpha_4)/2)}{\partial x_k}\Delta x\Delta y, \tag{A.2}$$

$$\frac{\partial p_{kl}}{\partial\beta_{x2}}\approx-\frac{1}{2}\frac{\partial G(x_k-(\alpha_3-\alpha_1)/2,y_l-(\alpha_4-\alpha_2)/2)}{\partial x_k}\Delta x\Delta y, \tag{A.3}$$

Since the distance $\delta$ is assumed to be small, Eqs. (A.2) and (A.3) can be Taylor expanded about $\alpha_1=0$ and $\alpha_2=0$ as follows:

$$\begin{aligned}\frac{\partial p_{kl}}{\partial\beta_{x1}}\approx-\frac{1}{2}\Bigg(&\frac{\partial G(x_k-\alpha_3/2,y_l-\alpha_4/2)}{\partial x_k}\\&-\frac{\alpha_1}{2}\frac{\partial^2G(x_k-\alpha_3/2,y_l-\alpha_4/2)}{\partial x_k^2}\\&-\frac{\alpha_2}{2}\frac{\partial^2G(x_k-\alpha_3/2,y_l-\alpha_4/2)}{\partial y_l\partial x_k}\Bigg)\Delta x\Delta y,\end{aligned} \tag{A.4}$$

$$\begin{aligned}\frac{\partial p_{kl}}{\partial\beta_{x2}}\approx-\frac{1}{2}\Bigg(&\frac{\partial G(x_k-\alpha_3/2,y_l-\alpha_4/2)}{\partial x_k}\\&+\frac{\alpha_1}{2}\frac{\partial^2G(x_k-\alpha_3/2,y_l-\alpha_4/2)}{\partial x_k^2}\\&+\frac{\alpha_2}{2}\frac{\partial^2G(x_k-\alpha_3/2,y_l-\alpha_4/2)}{\partial y_l\partial x_k}\Bigg)\Delta x\Delta y.\end{aligned} \tag{A.5}$$

Combining Eqs. (A.1), (A.4), and (A.5) results in

$$\begin{aligned}F_{11}-F_{12}\approx&\frac{N\Delta x\Delta y}{8}\sum_{k=1}^{K}\sum_{l=1}^{L}\\&\times\frac{\left(\alpha_1(\partial^2G(x_k-\alpha_3/2,y_l-\alpha_4/2)/\partial x_k^2)+\alpha_2(\partial^2G(x_k-\alpha_3/2,y_l-\alpha_4/2)/\partial y_l\partial x_k)\right)^2}{G(x_k-\alpha_3/2,y_l-\alpha_4/2)},\end{aligned} \tag{A.6}$$

where the denominator $p_{kl}$ has been approximated by $G(x_k-\alpha_3/2,y_l-\alpha_4/2)\Delta x\Delta y$, since the two components are assumed to overlap nearly completely. The following step is to substitute Eq. (5) into Eq. (A.6). Then, the sums can be approximated by integrals if it assumed that $\Delta x$ and $\Delta y$ are small. Straightforward calculations result in

$$F_{11}-F_{12}\approx\frac{N}{8\rho^4}(2\alpha_1^2+\alpha_2^2). \tag{A.7}$$

An analogous reasoning yields

$$F_{33}-F_{34}\approx\frac{N}{8\rho^4}(2\alpha_2^2+\alpha_1^2). \tag{A.8}$$

Next, it follows from Eq. (18) that

$$F_{13}-F_{14}\approx\frac{N}{2}\sum_{k=1}^{K}\sum_{l=1}^{L}\frac{1}{p_{kl}}\left(\frac{\partial p_{kl}}{\partial\beta_{x1}}-\frac{\partial p_{kl}}{\partial\beta_{x2}}\right)\left(\frac{\partial p_{kl}}{\partial\beta_{y1}}-\frac{\partial p_{kl}}{\partial\beta_{y2}}\right), \tag{A.9}$$

where it has been taken into account that $F_{13}\approx F_{24}$ and $F_{14}\approx F_{23}$. A similar derivation as that resulting in Eqs. (A.4) and (A.5) gives

$$\begin{aligned}\frac{\partial p_{kl}}{\partial\beta_{y1}}\approx-\frac{1}{2}\Bigg(&\frac{\partial G(x_k-\alpha_3/2,y_l-\alpha_4/2)}{\partial y_l}\\&-\frac{\alpha_1}{2}\frac{\partial^2G(x_k-\alpha_3/2,y_l-\alpha_4/2)}{\partial x_k\partial y_l}\\&-\frac{\alpha_2}{2}\frac{\partial^2G(x_k-\alpha_3/2,y_l-\alpha_4/2)}{\partial y_l^2}\Bigg)\Delta x\Delta y,\end{aligned} \tag{A.10}$$

$$\frac{\partial p_{kl}}{\partial \beta_{y2}} \approx -\frac{1}{2}\left(\frac{\partial G(x_k-\alpha_3/2, y_l-\alpha_4/2)}{\partial y_l} + \frac{\alpha_1}{2}\frac{\partial^2 G(x_k-\alpha_3/2, y_l-\alpha_4/2)}{\partial x_k \partial y_l} + \frac{\alpha_2}{2}\frac{\partial^2 G(x_k-\alpha_3/2, y_l-\alpha_4/2)}{\partial y_l^2}\right)\Delta x \Delta y. \quad (A.11)$$

The following step is combining Eqs. (5) and (A.9)–(A.11). In the thus obtained expression, the denominator $p_{kl}$ can be approximated by $G(x_k-\alpha_3/2, y_l-\alpha_4/2)\Delta x\Delta y$ and if $\Delta x$ and $\Delta y$ are assumed to be small, the sums can be approximated by integrals. This results in

$$F_{13} - F_{14} \approx \frac{N\alpha_1\alpha_2}{8\rho^4}. \quad (A.12)$$

Finally, substitution of Eqs. (A.7), (A.8), and (A.12) into Eq. (31) results in Eq. (32).

Second, Eq. (33), which is valid if $\delta$ is large compared to $\rho$, will be proven. From the assumption that the components do not overlap, it can be shown that the nondiagonal elements of $F$, which is given in Eq. (23), are approximately equal to zero. On the other hand, it can be shown that the diagonal elements of $F$ are nonzero and equal to one another. For example, it follows from Eq. (18) that:

$$F_{11} = N\sum_{k=1}^{K}\sum_{l=1}^{L}\frac{1}{p_{kl}}\frac{\partial p_{kl}}{\partial \beta_{x1}}\frac{\partial p_{kl}}{\partial \beta_{x1}}. \quad (A.13)$$

In this expression, $p_{kl}$ can be replaced by Eq. (7). Then, $g(x_k, y_l; \beta)$ can be replaced by Eqs. (4) and (5). From the assumption that the two components do not overlap, the denominator $p_{kl}$ can be approximated by $0.5G(x_k-\beta_{x1}, y_l-\beta_{y1})\Delta x\Delta y$. In the thus obtained expression, the sums are approximated by integrals, resulting in

$$F_{11} \approx \frac{N}{2\rho^2}. \quad (A.14)$$

An analogous reasoning results in the same approximations for the other diagonal elements of $F$. Substitution of these approximations into Eq. (31) results in Eq. (33).

## Appendix B

In this appendix, the approximations, given in Eqs. (39) and (40), for the highest attainable precision with which the distance between two components of a three-dimensional object can be estimated will be derived. First, Eq. (39), which is valid if $\delta$ is small compared to $\rho$, will be proven. From Eq. (18), it follows that

$$F_{11} - F_{12} \approx \frac{N}{2J}\sum_{j=1}^{J}\sum_{k=1}^{K}\sum_{l=1}^{L}\frac{1}{p'_{kl}}\left(\frac{\partial p^j_{kl}}{\partial \beta_{x1}} - \frac{\partial p^j_{kl}}{\partial \beta_{x2}}\right)^2, \quad (B.1)$$

where it has been taken into account that $F_{11} \approx F_{22}$ and $F_{12} = F_{21}$. The number of electrons $n$ and the summation over $m$ in Eq. (18) have been replaced by the number of electrons per projection $N/J$ and the summations over $j, k$, and $l$. According to the chain rule for differentiation and from Eq. (10), it follows that

$$F_{11} - F_{12} \approx \sum_{j=1}^{J}\frac{1}{J}\cos^2\theta^j \times \left[\frac{N}{2}\sum_{k=1}^{K}\sum_{l=1}^{L}\frac{1}{p^j_{kl}}\left(\frac{\partial p^j_{kl}}{\partial \beta^j_{x1}} - \frac{\partial p^j_{kl}}{\partial \beta^j_{x2}}\right)^2\right]. \quad (B.2)$$

From Eqs. (7), (11), and (12), it follows that the sum between squared brackets is equal to Eq. (A.1), if $\beta_{x1}$ and $\beta_{x2}$ in Eq. (A.1) are replaced by $\beta^j_{x1}$ and $\beta^j_{x2}$, respectively. Therefore, it can be replaced by the approximation of Eq. (A.1), which is given in Eq. (A.7), resulting in

$$F_{11} - F_{12} \approx \sum_{j=1}^{J}\frac{1}{J}\cos^2\theta^j \times \left[\frac{N}{8\rho^4}\left(2(\beta^j_{x1}-\beta^j_{x2})^2 + (\beta^j_{y1}-\beta^j_{y2})^2\right)\right]. \quad (B.3)$$

Substitution of Eq. (10) into Eq. (B.3) gives

$$F_{11} - F_{12} \approx \sum_{j=1}^{J}\frac{1}{J}\cos^2\theta^j \times \left[\frac{N}{8\rho^4}\left(2(\alpha_1\cos\theta^j + \alpha_3\sin\theta^j)^2 + (\alpha_2)^2\right)\right], \quad (B.4)$$

where the elements of the parameter $\alpha$ are given by Eq. (35). The projections $j$ are taken at the tilt angles $\theta^j, j = 1, \ldots, J$, which are assumed to be equidistantly sampled at the interval $(-\pi/2, \pi/2)$. In this case, the difference $\Delta\theta$ between successive tilt angles is equal to

$$\Delta\theta = \frac{\pi}{J}. \quad (B.5)$$

This expression can be substituted into Eq. (B.4). It will be assumed that $J$ is large, so that $\Delta\theta$ is small. In this way, $\sum_j \Delta\theta$ can be approximated by $\int d\theta$. Straightforward calculations yield

$$F_{11} - F_{12} \approx \frac{N}{16\rho^4}\left(\frac{3}{2}\alpha_1^2 + \alpha_2^2 + \frac{1}{2}\alpha_3^2\right). \quad (B.6)$$

Similar reasonings result in

$$F_{33} - F_{34} \approx \frac{N}{8\rho^4}\left(\frac{1}{2}\alpha_1^2 + 2\alpha_2^2 + \frac{1}{2}\alpha_3^2\right) \quad (B.7)$$

and

$$F_{55} - F_{56} \approx \frac{N}{16\rho^4}\left(\frac{1}{2}\alpha_1^2 + \alpha_2^2 + \frac{3}{2}\alpha_3^2\right). \quad (B.8)$$

Next, it follows from Eq. (18) that

$$F_{13}-F_{14}\approx\frac{N}{2J}\sum_{j=1}^{J}\sum_{k=1}^{K}\sum_{l=1}^{L}\frac{1}{p_{kl}^{j}}\times\left(\frac{\partial p_{kl}^{j}}{\partial\beta_{x1}}-\frac{\partial p_{kl}^{j}}{\partial\beta_{x2}}\right)\left(\frac{\partial p_{kl}^{j}}{\partial\beta_{y1}}-\frac{\partial p_{kl}^{j}}{\partial\beta_{y2}}\right),\tag{B.9}$$

where it has been taken into account that $F_{13}\approx F_{24}$ and $F_{14}\approx F_{23}$. A similar derivation as that resulting in Eq. (B.2) gives

$$F_{13}-F_{14}\approx\sum_{j=1}^{J}\frac{1}{J}\cos\theta^{j}\times\left[\frac{N}{2}\sum_{k=1}^{K}\sum_{l=1}^{L}\frac{1}{p_{kl}^{j}}\left(\frac{\partial p_{kl}^{j}}{\partial\beta_{x1}^{j}}-\frac{\partial p_{kl}^{j}}{\partial\beta_{x2}^{j}}\right)\times\left(\frac{\partial p_{kl}^{j}}{\partial\beta_{y1}^{j}}-\frac{\partial p_{kl}^{j}}{\partial\beta_{y2}^{j}}\right)\right].\tag{B.10}$$

From Eqs. (7), (11), and (12), it follows that the sum between squared brackets is equal to Eq. (A.9), if $\beta_{x1},\beta_{x2},\beta_{y1}$, and $\beta_{y2}$ in Eq. (A.9) are replaced by $\beta_{x1}^{j},\beta_{x2}^{j},\beta_{y1}^{j}$, and $\beta_{y2}^{j}$, respectively. Therefore, it can be replaced by the approximation of Eq. (A.9), which is given by Eq. (A.12)

$$F_{13}-F_{14}\approx\sum_{j=1}^{J}\frac{1}{J}\cos\theta^{j}\left[\frac{N(\beta_{x1}^{j}-\beta_{x2}^{j})(\beta_{y1}^{j}-\beta_{y2}^{j})}{8\rho^{4}}\right].\tag{B.11}$$

Substitution of Eq. (10) into Eq. (B.11) yields

$$F_{13}-F_{14}\approx\sum_{j=1}^{J}\frac{1}{J}\cos\theta^{j}\left[\frac{N(\alpha_{1}\cos\theta^{j}+\alpha_{3}\sin\theta^{j})(\alpha_{2})}{8\rho^{4}}\right],\tag{B.12}$$

where the elements of the parameter $\alpha$ are given in Eq. (35). Then, Eq. (B.5) can be substituted into Eq. (B.12). Assuming that $J$ is large results in

$$F_{13}-F_{14}\approx\frac{N}{16\rho^{4}}\alpha_{1}\alpha_{2}.\tag{B.13}$$

Similar reasonings yield

$$F_{15}-F_{16}\approx\frac{N}{16\rho^{4}}\alpha_{1}\alpha_{3}\tag{B.14}$$

and

$$F_{35}-F_{36}\approx\frac{N}{16\rho^{4}}\alpha_{2}\alpha_{3}.\tag{B.15}$$

Finally, Eqs. (B.6)–(B.8) and (B.13)–(B.15) can be substituted into Eq. (38). Furthermore, the distance $\delta'$ between the components projected onto the $(x,z)$-plane is equal to

$$\delta'=\sqrt{\alpha_{1}^{2}+\alpha_{3}^{2}}=\delta\sin\phi,\tag{B.16}$$

where $\phi$ is the angle between the rotation axis and the axis that connects the two components. The distance $\delta'$ and the angle $\phi$ are presented in Fig. 1.The distance $\alpha_2$ between the components projected onto the $(y,z)$-plane is equal to

$$\alpha_{2}=\delta\cos\phi.\tag{B.17}$$

Taking account of Eqs. (B.16) and (B.17) results in Eq. (39).

Second, Eq. (40), which is valid if $\delta$ is large compared to $\rho$, will be proven. From the assumption that the components do not overlap, it can be shown that the nondiagonal elements of $F$, which is given in Eq. (34), are approximately equal to zero. On the other hand, it can be shown that the diagonal elements of $F$ are nonzero. From Eq. (18), it follows that

$$F_{11}=\frac{N}{J}\sum_{j=1}^{J}\sum_{k=1}^{K}\sum_{l=1}^{L}\frac{1}{p_{kl}^{j}}\frac{\partial p_{kl}^{j}}{\partial\beta_{x1}}\frac{\partial p_{kl}^{j}}{\partial\beta_{x1}}.\tag{B.18}$$

According to the chain rule for differentiation and from Eq. (10), it follows that

$$F_{11}=\sum_{j=1}^{J}\frac{1}{J}\cos^{2}\theta^{j}\left[N\sum_{k=1}^{K}\sum_{l=1}^{L}\frac{1}{p_{kl}^{j}}\frac{\partial p_{kl}^{j}}{\partial\beta_{x1}^{j}}\frac{\partial p_{kl}^{j}}{\partial\beta_{x1}^{j}}\right].\tag{B.19}$$

From Eqs. (7), (11), and (12), it follows that the sum between squared brackets is equal to Eq. (A.13), if $\beta_{x1}$ in Eq. (A.13) is replaced by $\beta_{x1}^{j}$. If the distance between the two components in the projected image is large, it can be replaced by the approximation of Eq. (A.13), which is given in Eq. (A.14). This condition is fulfilled for most projections. However, even if the distance between the three-dimensional components is large, their projected distance can be small. Since it is assumed that the total number of projections is large, the contribution of projections for which this condition is not fulfilled can be neglected. Therefore, Eq. (B.19) can be approximated as follows:

$$F_{11}\approx\sum_{j=1}^{J}\frac{1}{J}\cos^{2}\theta^{j}\frac{N}{2\rho^{2}}.\tag{B.20}$$

Then, Eq. (B.5) can be substituted into Eq. (B.20) and $\sum_j\Delta\theta$ can be approximated by $\int\mathrm{d}\theta$, yielding

$$F_{11}\approx\frac{N}{4\rho^{2}}.\tag{B.21}$$

Analogous reasonings result in

$$F_{33}\approx\frac{N}{2\rho^{2}}\tag{B.22}$$

and

$$F_{55}\approx\frac{N}{4\rho^{2}}.\tag{B.23}$$

Substitution of these approximations into Eq. (38) and making use of Eqs. (37) and (B.16) results in Eq. (40).

## References

Baumeister, W., Steven, A.C., 2000. Macromolecular electron microscopy in the era of structural genomics. Trends Biochem. Sci. 25, 624–631.

Bettens, E., Van Dyck, D., den Dekker, A.J., Sijbers, J., van den Bos, A., 1999. Model-based two-object resolution from observations having counting statistics. Ultramicroscopy 77, 37–48.

Crowther, R.A., DeRosier, D.J., Klug, A., 1970. The reconstruction of a three-dimensional structure from projections and its application to electron microscopy. Proc. R. Soc. London A 317, 319–340.

den Dekker, A.J., van den Bos, A., 1997. Resolution: a survey. J. Opt. Soc. Am. A 14, 547–557.

den Dekker, A.J., Sijbers, J., Van Dyck, D., 1999. How to optimize the design of a quantitative HREM experiment so as to attain the highest precision. J. Microsc. 194, 95–104.

Grimm, R., Singh, H., Rachel, R., Typke, D., Zillig, W., Baumeister, W., 1998. Electron tomography of ice-embedded prokaryotic cells. Biophys. J. 74, 1031–1042.

Hegerl, R., Hoppe, W., 1976. Influence of electron noise on three-dimensional image reconstruction. Z. Naturforsch. A31, 1717–1721.

Mood, A.M., Graybill, F.A., Boes, D.C., 1974. Introduction to the Theory of Statistics, third ed. McGraw-Hill, Tokyo.

Radermacher, M., 1992. Weighted back-projection methods. In: Frank, J. (Ed.), Electron Tomography—Three-dimensional Imaging with the Transmission Electron Microscope. Plenum, New York/London, pp. 91–115.

Rayleigh, Lord, 1902. Wave theory of light. In: Scientific Papers by John William Strutt, Baron Rayleigh, vol. 3. Cambridge University Press, Cambridge, UK, 47–189.

van den Bos, A., 1982. Parameter estimation. In: Sydenham, P.H. (Ed.), Handbook of Measurement Science, vol. 1. Wiley, Chicester, UK, pp. 331–377.

van den Bos, A., den Dekker, A.J., 2001. Resolution reconsidered—conventional approaches and an alternative. In: Hawkes, P.W. (Ed.), Advances in Imaging and Electron Physics, vol. 117. Academic Press, San Diego, pp. 241–360.